Journal of Sound and Vibration (1999) **225**(1), 153–170
Article No. jsvi.1999.2228, available online at http://www.idealibrary.com on IDEAL®

DYNAMIC BENDING AND TORSION STIFFNESS DERIVATION FROM MODAL CURVATURES AND TORSION RATES

J. MAECK AND G. DE ROECK

Department of Civil Engineering, Division of Structural Mechanics, K.U. Leuven, W. de Croylaan 2, *B*-3001 *Heverlee, Belgium*

(*Received* 11 *August* 1998, *and in final form* 26 *February* 1999)

In order to maintain the reliability of civil engineering structures, considerable effort is currently spent on developing a non-destructive vibration testing method for monitoring the structural integrity of constructions. The technique must be able to observe damage, secondly to localize the damage; and finally to give an idea of the severity of the damage. Within the framework of relating changes of measured modal parameters to changes in the integrity of the structure, it is important to be able to determine the dynamic stiffness in each section of the structure from measured modal characteristics.

A damaged structure results in a dynamic stiffness reduction of the cracked sections. The dynamic stiffnesses provide directly an indication of the extension of the cracked zones in the structure. The dynamic stiffness reduction can also be associated with a degree of cracking in a particular zone.

In an experimental programme, a concrete beam of 6 m length is subjected to an increasing static load to produce cracks. After each static perload, the beam is tested dynamically in a free–free set-up. The change in modal parameters is then related to damage in the beam.

The technique that will be presented in the paper to predict the damage location and intensity is a direct stiffness derivation from measured modal displacement derivatives. Using the bending modes, the dynamic bending stiffness can be derived from modal curvatures. Using the torsional modes, the dynamic torsion stiffness can be derived from modal torsion rates.

1. INTRODUCTION

In the framework of developing a non-destructive vibration testing method for monitoring the structural integrity of constructions in civil engineering, a technique is elaborated to derive the dynamic bending and torsion stiffness at a certain location of a structure using the measured mode shapes and the corresponding eigenfrequencies. One of the goals of non-destructive vibration testing is to relate a shift in measured modal characteristics to a change in material properties of the structure.

0022-460X/99/310153 + 18 $30.00/0

Determining the damage parameters from modal parameter shifts belongs to the group of inverse problems [1]. Many studies have attempted to determine and localize damage patterns only from changes of eigenfrequencies [2, 3]. Even though eigenfrequencies are sensitive indicators of structural integrity [4], methods using only eigenfrequencies have a number of shortcomings. They cannot distinguish damage at symmetrical locations in a symmetric structure, and the number of measured eigenfrequencies is generally lower than the number of unknown modal parameters resulting in a non-unique solution. Therefore, also mode shapes can be included in damage detection. In references [5, 6] changes in strain energy are used to localize damage, while Ruotolo and Surace [7] fit a mathematical model to measurements by minimizing an objective function. In reference [8] expressions relating variations in stiffness of structural elements to the variations in modal stiffness are generated, resulting in a system of algebraic equations with known fractional changes in modal stiffness and unknown fractional changes in member stiffness. However, modal displacements are rather insensitive to moderate damage. Pandey *et al.* [9] introduce curvature mode shapes. Modal curvatures seem to be locally much more sensitive to damage than modal displacements [10]. Accurate estimation of the curvatures from experimental data remains difficult. In the paper, a technique is developed to calculate the modal curvatures and torsion rates without numerical derivation from the displacements. Combined with modal internal forces this leads directly to an estimation of stiffness decrease in the structure.

After a description of the test set-up, the direct stiffness derivation procedure is explained. The technique is then validated using experimental data.

2. TEST PROGRAM

An experimental programme was set up to establish the relation between damage and changes of the dynamic system characteristics. In the test programme, a reinforced concrete beam of 6 m length is subjected to an increasing static load in order to produce cracks.

The test beam is subjected to two identical point loads (symmetric at 1 m from the middle). After each loadstep (6 in total, Table 1), an experimental modal

TABLE 1

Static loadsteps

	Static load (kN)
Step 0 (reference)	0
Step 1	4
Step 2	6
Step 3	12
Step 4	18
Step 5	24
Step 6	25·3

analysis is performed on the beam. The last loadstep (6 in total, Table 1), an experimental modal analysis is performed on the beam. The last loadstep corresponds to failure (plastic yielding of the reinforcement bars).

A free–free set-up for the beam is established by using very flexible springs to support the beam. Accelerometers were placed at 20 cm intervals along both longitudinal edges of the upper side of the beam (62 measurement points in total). The experimental set-up and beam characteristics are given in Figures 1 and 2 [11]: $\varnothing 8$ denotes the diameter of the stirrups, placed every 200 mm, whereas $\varnothing 16$ is the diameter of the longitudinal rebars, running the full length of the beam.

The stochastic subspace identification technique is applied to the dynamic response of the beam in order to extract the modal parameters [11, 12]. The first three bending modes and the first torsional mode are plotted in Figure 3. To visualize the torsional mode, the vertical deflections at both longitudinal edges of the upper side of the beam are shown.

In Figure 4 the observed crack pattern and growth is shown for the successive static loadsteps.

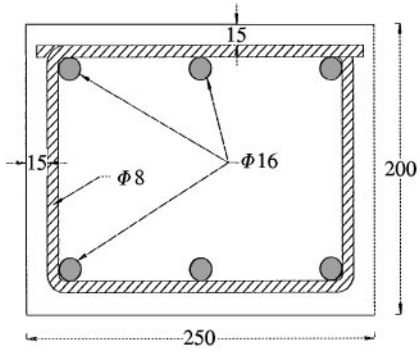

Figure 1. Section characteristics.

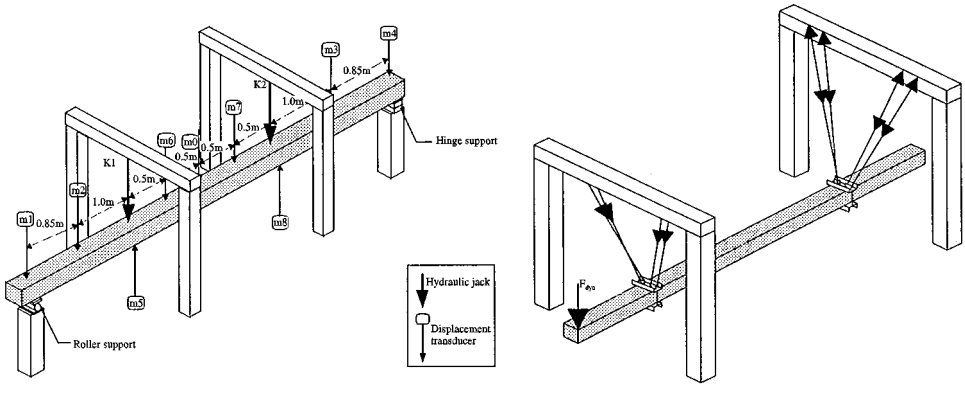

Figure 2. Static & dynamic set-up.

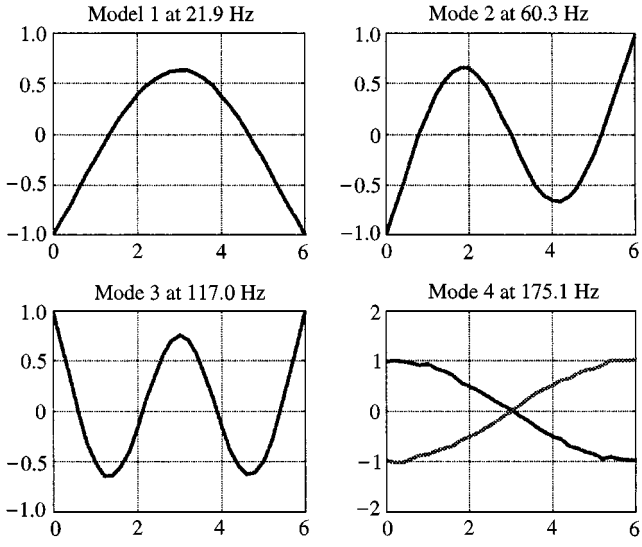

Figure 3. First four identified mode shapes.

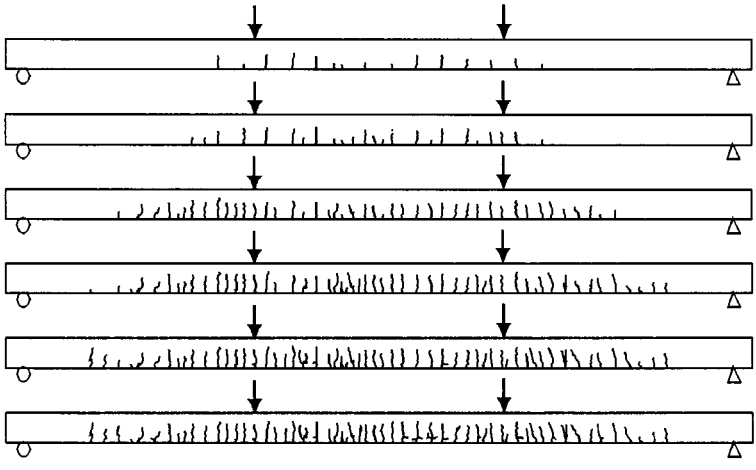

Figure 4. Crack pattern for six loadsteps.

3. SOLUTION PROCEDURE

The direct dynamic stiffness calculation uses the experimental mode shapes in deriving the dynamic stiffness. If the mass distribution is assumed to be known, the great advantage is that no numerical model is needed to obtain the dynamic stiffness distribution for statically determined structures. For hyperstatic structures, the reaction forces and consequently the internal forces are dependent on the stiffness of the structure. Therefore, an iterative procedure is applied to a numerical model to find the bending stiffness distribution of a hyperstatic structure.

The method makes use of the basic relation that the dynamic bending stiffness (EI) in each section is equal to the bending moment (M) in that section divided by the corresponding curvature (second derivative of bending mode φ^b). In the same

manner, the dynamic torsion stiffness (GJ) in each section is equal to the torsional moment (T) in that section divided by the corresponding torsion rate (or torsion angle per unit length, i.e. first derivative of torsional mode φ^t):

$$EI = \frac{M}{\mathrm{d}^2\varphi^b/\mathrm{d}x^2},$$

$$GJ = \frac{T}{\mathrm{d}\varphi^t/\mathrm{d}x}. \tag{1}$$

4. CALCULATION OF MODAL INERTIA FORCES

The eigenvalue problem of the undamped system can be written as

$$\mathbf{K}_m \boldsymbol{\varphi}_m = \omega_m^2 \mathbf{M}_a \boldsymbol{\varphi}_m, \tag{2}$$

in which $\mathbf{K}_m$ is the stiffness matrix, $\mathbf{M}_a$ the analytical mass matrix, $\boldsymbol{\varphi}_m$ the vector of the measured modal displacements and ω_m the measured eigenpulsation. This can be seen as a pseudo-static system: for each mode internal (section) forces are due to the inertial load which can be calculated as the product of local mass and local acceleration ($= \omega_m^2 \cdot \boldsymbol{\varphi}_m$).

The mass distribution is assumed to be known. A lumped mass matrix is used in equation (2), which is acceptable if the measurement mesh is rather dense.

For the bending modes $\boldsymbol{\varphi}_m$ is equal to $\boldsymbol{\varphi}_m^b$, the vertical deflections that are directly available. In the calculation of the modal internal forces, the contribution of rotational inertia is proven to be negligible for the lower modes. For the torsional modes, $\boldsymbol{\varphi}_m$ is equal to $\boldsymbol{\varphi}_m^t$, and the rotation angles are not directly measured but are, in the case of the beam, easily obtained from the vertical deflections on both sides of the beam.

If in equation (2), $\boldsymbol{\varphi}_m$ contains only the modal displacements at the measurement points, one obtains a discrete pattern of the inertia load. A correction can be made by linearly interpolating the measurements and obtaining in this way a distributed load.

From now on $\boldsymbol{\varphi}_m$ (and $\boldsymbol{\varphi}_m^b$ and $\boldsymbol{\varphi}_m^t$) denotes the continuous mode shape, i.e. the piecewise linear function through the measurement points at location x_i, x_{i+1}, etc.

5. CALCULATION OF MODAL INTERNAL FORCES

From the modal inertia load the shear forces (V_i), the bending moments (M_i) and torsional moments (T_i), needed to evaluate (1) can now be calculated at each section. The sign convention is denoted in Figure 5.

$$M_{i+1} = M_i + T_i(x_{i+1} - x_i) - \int_{x_i}^{x_{i+1}} \omega_m^2 \rho A \varphi_m^b(x)(x_{i+1} - x)\,\mathrm{d}x$$

$$= M_i + T_i(x_{i+1} - x_i) - \omega_m^2 \rho A \int_{x_i}^{x_{i+1}} \left[\frac{\varphi_{m,i+1}^b - \varphi_{m,i}^b}{x_{i+1} - x_i}(x - x_i) + \varphi_{m,i}^b\right](x_{i+1} - x)\,\mathrm{d}x,$$

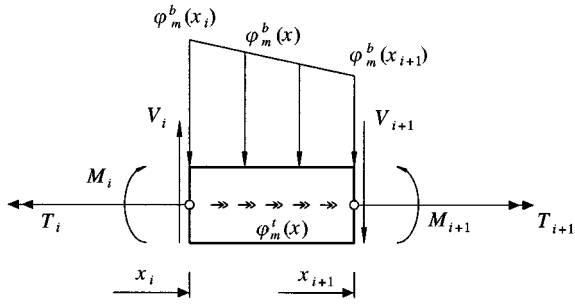

Figure 5. Sign convention for internal forces and displacements.

$$V_{i+1} = V_i - \int_{x_i}^{x_{i+1}} \omega_m^2 \rho A \varphi_m^b(x)\,\mathrm{d}x$$

$$= V_i - \omega_m^2 \rho A\,(\varphi^b_{m,i+1} - \varphi^b_{m,i})\,\frac{x_{i+1} - x_i}{2},$$

$$T_{i+1} = T_i - \int_{x_i}^{x_{i+1}} \omega_m^2\, i_\alpha\, \varphi_m^t(x)\,\mathrm{d}x$$

$$= T_i - \omega_m^2\, \rho\, \frac{a^2 + b^2}{12}\,(\varphi^t_{m,i+1} - \varphi^t_{m,i})\,\frac{x_{i+1} - x_i}{2}. \tag{3}$$

In equation (3), ρ, A, i_α, a, b are respectively the density, cross-sectional area, polar moment of inertia and the height and width of the beam. The values for V_0, M_0 and T_0 are zero in the recursive formula (3). Because of the free–free set-up in the dynamic tests, the inertia forces should be in static equilibrium. Due to measurement errors, this is not exactly the case, which causes non-uniqueness of the internal forces. Therefore, a Gram–Schmidt orthogonalization will be applied to the experimental mode shapes. The corrected mode $\boldsymbol{\varphi}_m^N$ for bending and torsional modes can be calculated from

$$\boldsymbol{\varphi}_m^{b,N} = \boldsymbol{\varphi}_m^b + aX_1 + bX_2,$$

$$\boldsymbol{\varphi}_m^{t,N} = \boldsymbol{\varphi}_m^t + cX_3, \tag{4}$$

with a, b and c being the unknowns to be determined from the vertical, moment and torsional equilibrium:

$$\omega_m^2\, \rho A \int_{-1/2}^{1/2} (\boldsymbol{\varphi}_m^b + aX_1 + bX_2)\,\mathrm{d}x = 0,$$

$$\omega_m^2\, \rho A \int_{-1/2}^{1/2} (\boldsymbol{\varphi}_m^b + aX_1 + bX_2)x\,\mathrm{d}x = 0,$$

$$\omega_m^2\, i_\alpha \int_{-1/2}^{1/2} (\boldsymbol{\varphi}_m^t + cX_3)\,\mathrm{d}x = 0. \tag{5}$$

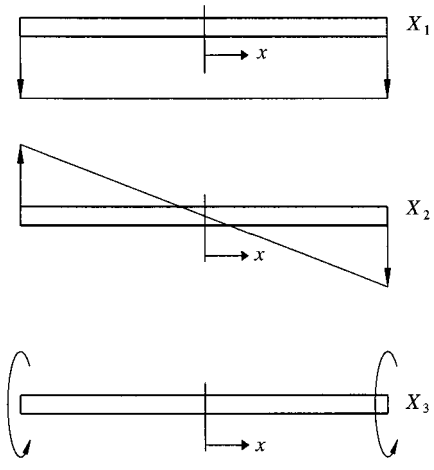

Figure 6. Three rigid-body modes of free–free beam.

X_1, X_2, X_3 are respectively the translational and two rotational rigid-body modes of the free beam (Figure 6).

Equation (5) in fact states nothing more than that the bending and torsional modes are mass-orthogonal to respectively X_1, X_2 and X_3, i.e.

$$X_1^T \mathbf{M}_a \boldsymbol{\varphi}_m^{b,N} = 0,$$

$$X_2^T \mathbf{M}_a \boldsymbol{\varphi}_m^{b,N} = 0,$$

$$X_3^T \mathbf{M}_a \boldsymbol{\varphi}_m^{t,N} = 0. \tag{6}$$

Using now in equation (3) the orthogonalized mode shapes (4), the internal modal forces can uniquely be calculated in each section.

6. DETERMINATION OF CURVATURES AND TORSION RATES

The next step in deriving the dynamic bending and torsion stiffness consists of the calculation of curvatures along the beam for the bending modes and torsion rates for the torsional modes. Direct calculation of first and second derivatives from measured mode shapes, e.g. by using the central difference approximation, results in oscillating and inaccurate values. A smoothing procedure accounting for the inherent inaccuracies of the measured mode shapes should be applied.

A first step in smoothing the mode shapes is called global smoothing. Measured deflections (or derived rotation angles in the case of a torsional mode) are fitted in a least-squares sense by a polynomial of a degree high enough to give a close approximation of the measured mode shapes but certainly lower than the number of measurement points to smooth out the errors. The optimal degree of the fitting polynomial increases for higher modes.

A difficult point is to choose an appropriate degree for the polynomial. If too low a degree is chosen the measurements are smoothed too much; if too high a degree is chosen measurement errors are not filtered out.

Also an alternative smoothing procedure, i.e. a weighted residual penalty-based technique, has been established.

For the bending modes one is interested to obtain the second derivatives of the modal deflections [equation (1)]. The beam is divided into a number of elements separated by nodes corresponding to the measurement points. Each node has three degrees of freedom: the modal vertical displacement v, the modal rotation ψ and the modal curvature κ, which are approximated independently (Figure 7). Linear shape functions N_i are used.

This is analogous to the Mindlin plate element, for which the rotations are approximated independently from the deflection. For this reason, this method will be called the Mindlin approach.

The objective function, which has to be minimized, contains the difference between approximations and measured mode shapes. Two penalty terms are added to enforce continuity of rotations and curvatures in a mean, smeared way:

$$\pi = \int \frac{(v - \varphi_m^b)^2}{2}\,\mathrm{d}x + \frac{\alpha L^{e2}}{2}\int\left(\psi - \frac{\mathrm{d}v}{\mathrm{d}x}\right)^2 \mathrm{d}x + \frac{\beta L^{e4}}{2}\int\left(\kappa - \frac{\mathrm{d}\psi}{\mathrm{d}x}\right)^2 \mathrm{d}x, \qquad (7)$$

where φ_m^b denotes the measured mode shape, and L^e is the length of a finite element. Elements are chosen in such a way that nodes coincide with measurement points.

The first term states that the average difference between approximation and measurement has to be minimized. Without any other terms in the potential function, one will find a (piecewise linear) approximation through all measurement points. In order to filter experimental errors and so smooth the deflection, two extra terms are added. Differences between the (independent) approximations of rotations and curvatures with respectively the first derivatives of displacements and rotations are minimized. The coupling between the independently approximated unknown is established by these constraint conditions. The weight of these extra conditions is set by the dimensionless penalty factors α and β.

Deriving the objective function (7) to the unknown modal degrees of freedom gives the following equations from which displacements, rotations and curvatures

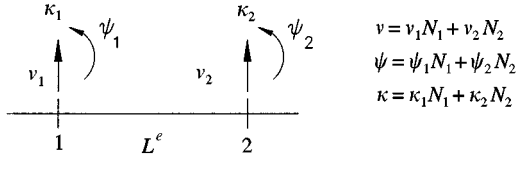

Figure 7. Element degrees of freedom.

are obtained:

$$\frac{\partial \pi}{\partial v_1} = 0 \mapsto \int N_1(v - \varphi_m)\,\mathrm{d}x + \alpha L^e \int \left(\psi - \frac{v_2 - v_1}{L^e}\right)\mathrm{d}x = 0,$$

$$\frac{\partial \pi}{\partial v_2} = 0 \mapsto \int N_2(v - \varphi_m^b)\,\mathrm{d}x - \alpha L^e \int \left(\psi - \frac{v_2 - v_1}{L^e}\right)\mathrm{d}x = 0,$$

$$\frac{\partial \pi}{\partial \psi_1} = 0 \mapsto \alpha L^{e2} \int N_1 \left(\psi - \frac{v_2 - v_1}{L^e}\right)\mathrm{d}x + \beta L^{e3} \int \left(\kappa - \frac{\psi_2 - \psi_1}{L^e}\right)\mathrm{d}x = 0,$$

$$\frac{\partial \pi}{\partial \psi_2} = 0 \mapsto \alpha L^{e2} \int N_2 \left(\psi - \frac{v_2 - v_1}{L^e}\right)\mathrm{d}x - \beta L^{e3} \int \left(\kappa - \frac{\psi_2 - \psi_1}{L^e}\right)\mathrm{d}x = 0,$$

$$\frac{\partial \pi}{\partial \kappa_1} = 0 \mapsto \beta L^{e4} \int N_1 \left(\kappa - \frac{\psi_2 - \psi_1}{L^e}\right)\mathrm{d}x = 0,$$

$$\frac{\partial \pi}{\partial \kappa_2} = 0 \mapsto \beta L^{e4} \int N_2 \left(\kappa - \frac{\psi_2 - \psi_1}{L^e}\right)\mathrm{d}x = 0, \tag{8}$$

Substituting the linear shape functions and solving the integral expressions gives an analytical form for the governing system on element level:

$$\begin{bmatrix}
\frac{L^e}{3} + \alpha L^e & \frac{L^e}{6} - \alpha L^e & \frac{\alpha L^{e2}}{2} & \frac{\alpha L^{e2}}{2} & 0 & 0 \\
 & \frac{L^e}{3} + \alpha L^e & -\frac{\alpha L^{e2}}{2} & -\frac{\alpha L^{e2}}{2} & 0 & 0 \\
 & & \frac{\alpha L^{e3}}{3} + \beta L^{e3} & \frac{\alpha L^{e3}}{3} - \beta L^{e3} & \frac{\beta L^{e4}}{2} & \frac{\beta L^{e4}}{2} \\
 & & & \frac{\alpha L^{e3}}{3} + \beta L^{e3} & -\frac{\beta L^{e4}}{2} & -\frac{\beta L^{e4}}{2} \\
 & \textit{Symm.} & & & \frac{\beta L^{e5}}{3} & \frac{\beta L^{e5}}{6} \\
 & & & & & \frac{\beta L^{e5}}{3}
\end{bmatrix}
\begin{bmatrix} v_1 \\ v_2 \\ \psi_1 \\ \psi_1 \\ \kappa_1 \\ \kappa_2 \end{bmatrix} =
\begin{bmatrix} \frac{\varphi_{m1} L^e}{3} + \frac{\varphi_{m2} L^e}{6} \\ \frac{\varphi_{m1} L^e}{3} + \frac{\varphi_{m2} L^e}{3} \\ 0 \\ 0 \\ 0 \\ 0 \end{bmatrix} \tag{9}$$

After assemblage, a symmetric, non-singular system of the order of three times the number of nodes is obtained.

Advantages of this Mindlin approach is that directly curvatures are available, boundary conditions can be imposed easily (in this experimental set-up curvatures at the free beam ends have to be zero) and the approximated modal deflections have not to go through all measurement points. A drawback is the difficulty in choosing appropriate penalty factors. Values which are too high cause locking of the system.

In the following, α and β are chosen in such a way that the median of the relative error on the modal deflections is 2–3%, which is a reasonable estimation of the anticipated measurement inaccuracy. Hence, every mode shape has its own penalty factors.

For the torsional modes the method adopted is similar. In equation (7), φ_m^b has to be replaced by φ_m^t and v, ψ and κ are now respectively the approximations for the rotation angles, the rotation angles per unit length and the second derivatives of the rotation angles. In the later calculation, only the first derivative is needed for torsion stiffness derivation. Approximating the second derivatives is not strictly necessary but turns out to have a positive effect on the smoothness of the first derivatives. For the free–free beam the boundary conditions are that the rotation angles per unit length are zero at the beam ends.

7. EXPERIMENTAL VALIDATION

In this section, the method will be validated by deriving the dynamic stiffness along the beam length. The results of the test programme will be used to evaluate the dynamic stiffness at successive damage states.

All numerical results are obtained from routines developed in the MATLAB [13] environment. The measured dynamic Young's modulus by an axial resonance test on a cylinder is 33,000 N/mm^2. Using the section dimensions (Figure 1), the bending stiffness for the test beam in the undamaged state is calculated to be $6{\cdot}46 \times 10^6$ N m^2. The torsion stiffness in the undamaged state is calculated to be $4{\cdot}75 \times 10^6$ N m^2, which corresponds to a shear modulus of 14,100 N/mm^2. All identified mode shapes are scaled to a value one as maximal modal displacement.

Making use of the pure measurements and calculating directly the second derivatives using the central difference approximation gives too much scatter as shown for the reference state (without any static preload) in Figure 8.

In the same way, using the first torsion mode, inaccurate torsion rates are obtained when using the finite-difference approximation. Torsion rates are not zero at the beam ends. One can also observe from Figure 9 that the over- or under-estimation of the angles along the beam for the different loadsteps is systematic, probably due to the lack of perfect verticality of the accelerometers on the beam surface.

When global smoothing is applied to the mode shapes, the obtained polynomial is derived twice to obtain the curvatures for bending modes and once to obtain the torsion rates for the torsion modes. This results in much smoother values (Figures 10 and 11).

The zero boundary conditions at the ends are quite well satisfied. It also turns out that the degree of the fitting polynomial influences the degree of distortion by outliers in the measurements.

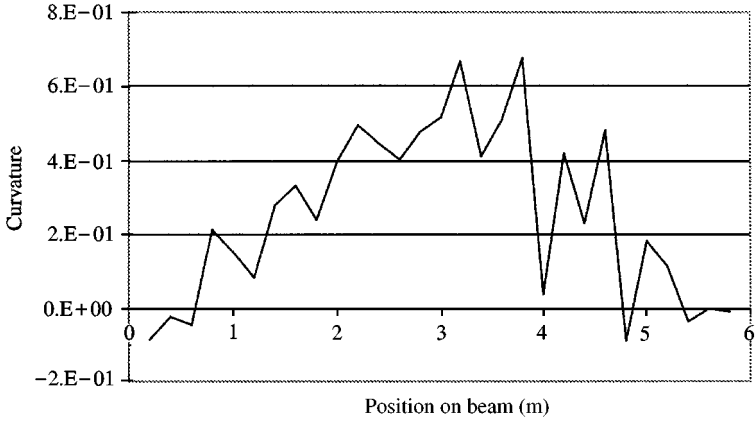

Figure 8. Curvatures for first bending mode—central difference approximation.

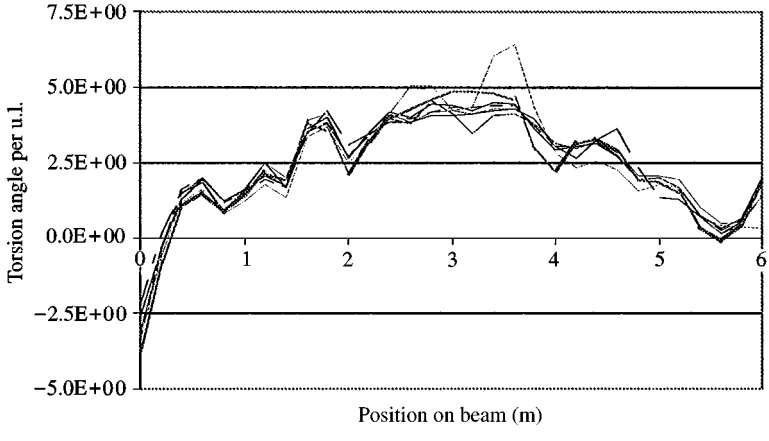

Figure 9. Torsion rates for first torsion mode—central difference approximation. —— Step 0; —– Step 1; – – – Step 2; —– – Step 3; ····· Step 4; ····· Step 5; ····· Step 6.

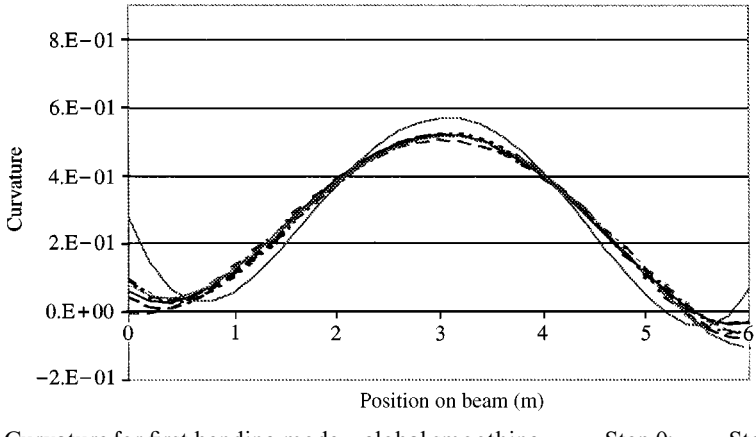

Figure 10. Curvature for first bending mode—global smoothing. —— Step 0; – – – Step 1; - - - Step 2; –·–·– Step 3; –··–··– Step 4; ····· Steps 5 and 6.

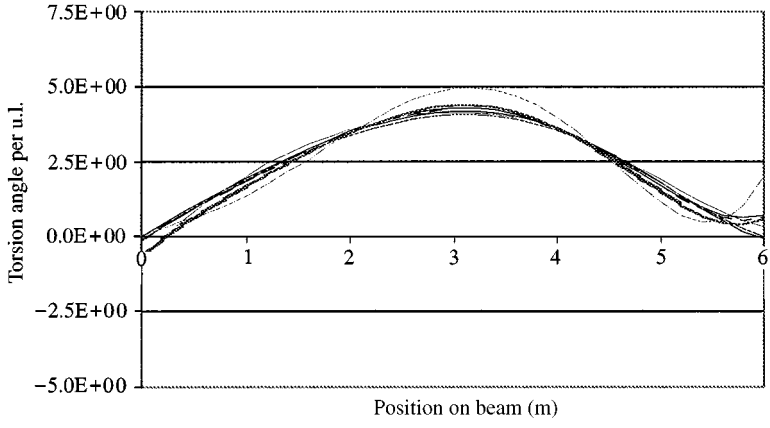

Figure 11. Torsion rates for first torsion mode—global smoothing. —— Step 0; —– Step 1; – – – Step 2; —–– Step 3; ····· Step 4; ····· Steps 5 and 6.

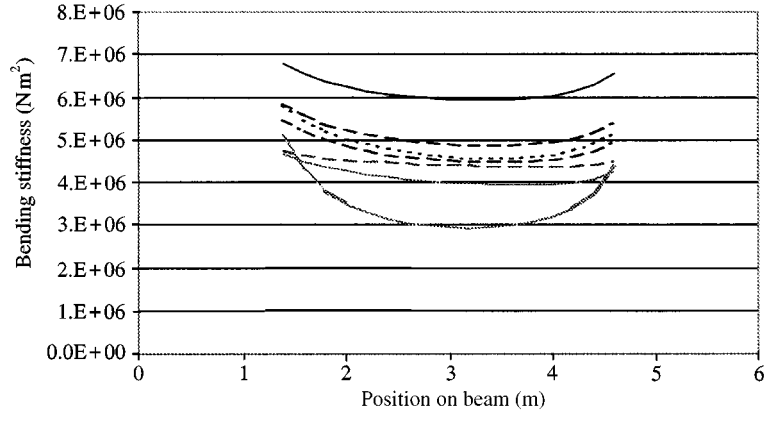

Figure 12. Bending stiffness for all loadsteps (first mode)—global smoothing. —— Step 0; – – – Step 1; - - - Step 2; –·–·– Step 3; –··–··– Step 4; ····· Steps 5 and 6.

As damage generally corresponds to a local increase in curvature, one should also take care not to conceal this change by the global polynomial. The main difficulty of the global smoothing technique is choosing an optimal degree.

Using the first bending and torsion mode, the stiffness reduction is shown in Figures 12 and 13.

The estimates are reliable within the interval 1·4–4·6 m. Outside this interval, estimates are inaccurate due to numerical inaccuracy near the beam ends (zero by zero division).

For the Mindlin approach the calculation procedure for the derivation of the modal curvatures is illustrated by Figure 14, which shows for the first mode shape the different finite-element variables along the beam axis in the reference (undamaged) state. Figure 14(a) shows the approximated versus the experimental mode shape (+), Figure 14 (b) the relative error with median value 2·1%, and Figures 14(c) and (d) the modal rotations and curvatures.

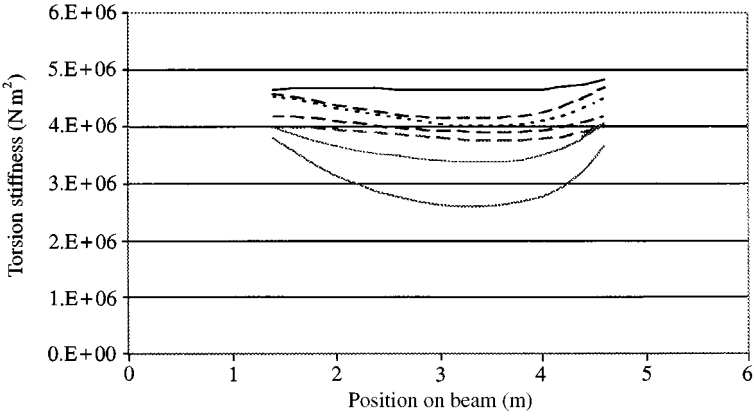

Figure 13. Torsion stiffness for all loadsteps (fourth mode)—global smoothing. —— Step 0; – – – Step 1; - - - Step 2; –·–·– Step 3; –··–··– Step 4; ····· Steps 5 and 6.

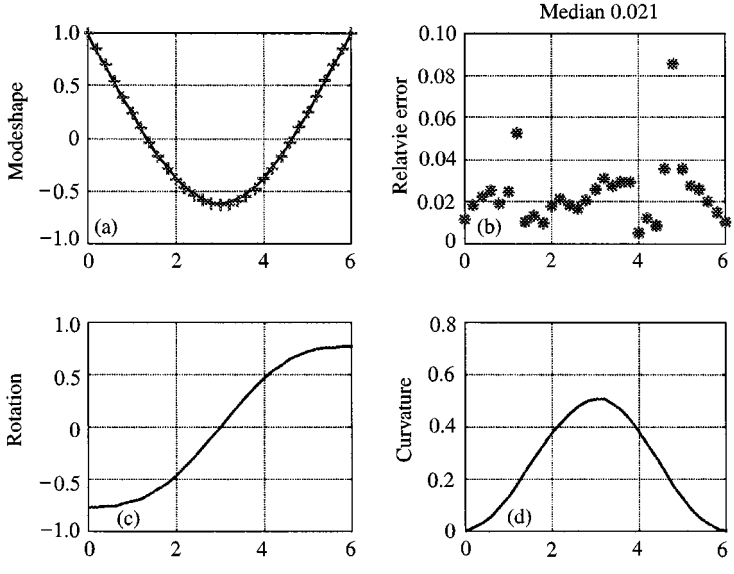

Figure 14. (a) Displacements v versus φ_m, for first bending mode—Mindlin approach. (b) Relative error, (c) rotations ψ, (d) curvatures κ.

To obtain the dynamic bending stiffness for the reference state, one should calculate the bending moments. Figure 15 shows the results for the first bending mode. Figure 15(a) shows the measured and the (almost identical) orthogonalized mode shape according to equation (4), plotted upon each other. Figure 15(b) shows the distributions of inertia forces from which the modal shear forces and bending moments can be determined according to equation (3) [Figures 15(c) and (d)]. Dividing the bending moments by the modal curvatures [Figure 15(e) identical to Figure 14(d)] results in the dynamic bending stiffness [Figure 15(f)].

From Figure 15 it can be noted that at the sections of almost-zero bending moments (or almost-zero curvatures), the approximation for EI is no longer

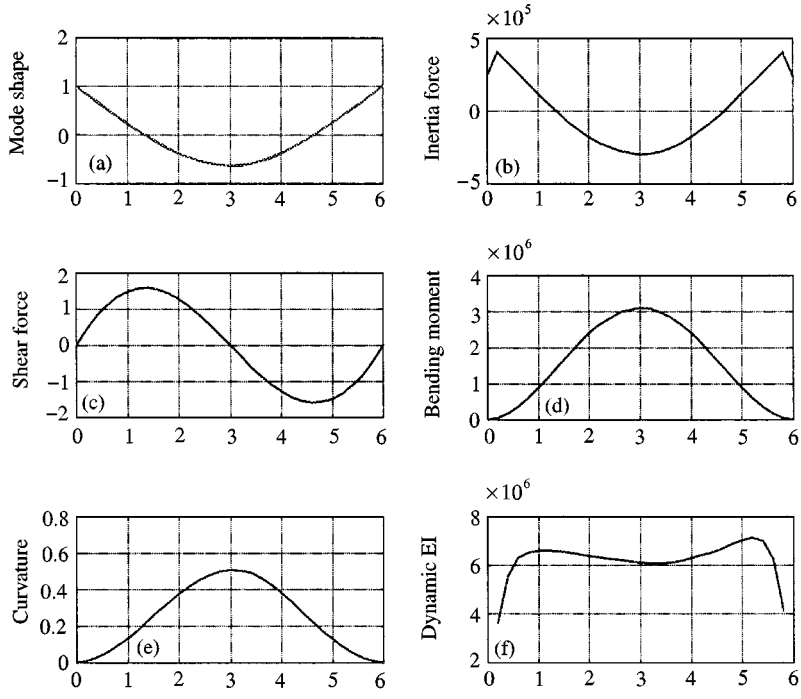

Figure 15. (a) Displacements first bending mode of beam, (b) inertia forces, (c) shear forces, (d) bending moments, (e) curvatures, (f) bending stiffness.

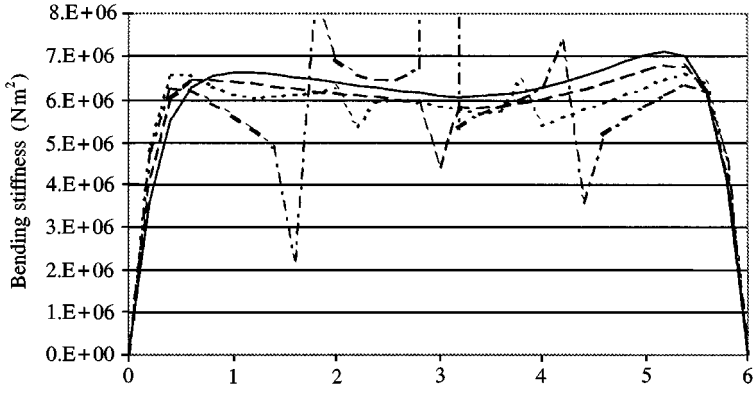

Figure 16. EI for first four bending modes—Mindlin approach. —— Mode 1; – – – Mode 2; - - - Mode 3; –-–- Mode 4.

accurate. Higher modes have even more sections with zero curvatures (Figure 16). This is a disadvantage when using the method for higher modes.

In the previous Figures, the dynamic stiffness is determined for the undamaged reference state of the beam. The same procedure can be followed for the measured modes and eigenfrequencies after each static loadstep in order to examine the stiffness degradation due to cracks in the beam. The evolution of the dynamic

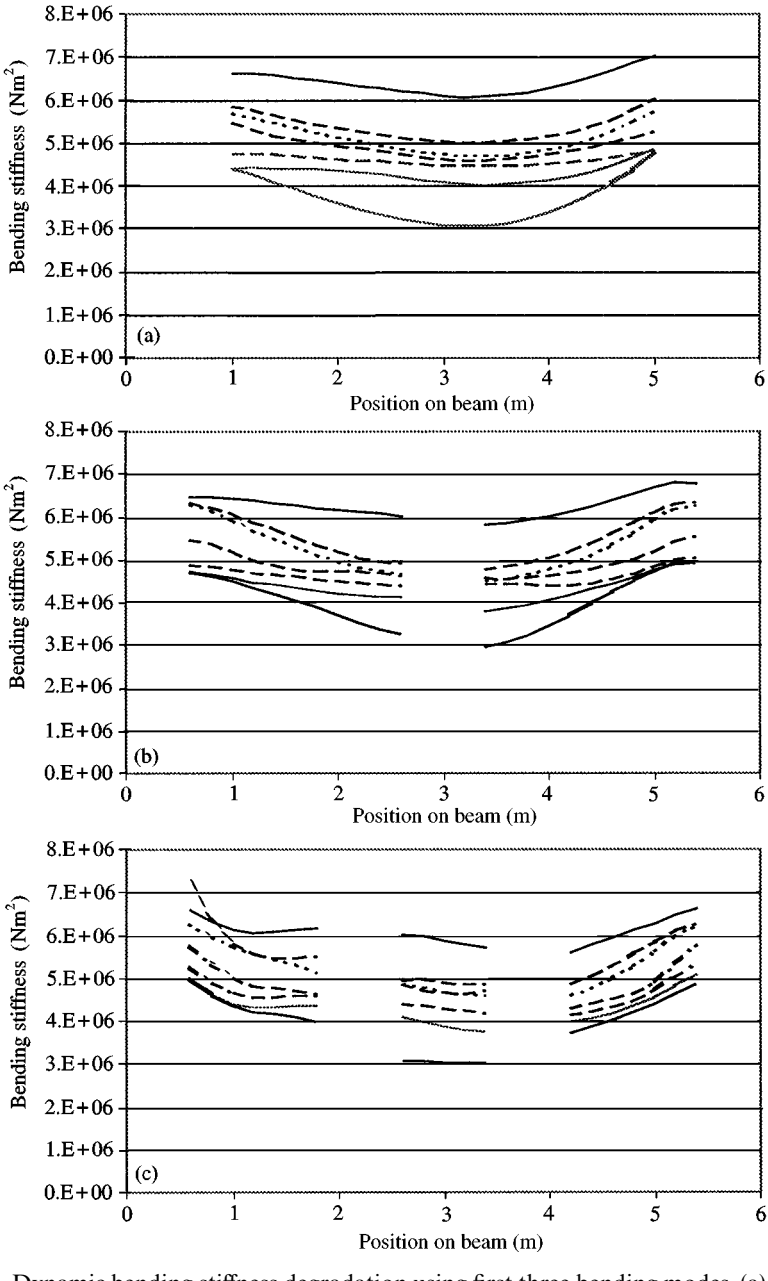

Figure 17. Dynamic bending stiffness degradation using first three bending modes. (a) —— Step 0; – – – Step 1; - - - Step 2; – – – – Step 3; – – – – – – Step 4; ····· Steps 5 and 6; (b) —— Step 0; – – – Step 1; - - - Step 2; – – – – Step 3; – – – – – – Step 4; ····· Steps 5 and 6; (c) —— Step 0; – – – Step 1; - - - Step 2; – – – – Step 3; – – – – – – Step 4; ····· Steps 5 and 6.

bending stiffness through different loadsteps is shown in Figure 17. In each plot information of one mode is used. In each Figure, the inaccurate zones due to almost zero bending moments and curvatures are omitted. Figure 18 shows the degradation of torsion stiffness using the first torsional mode.

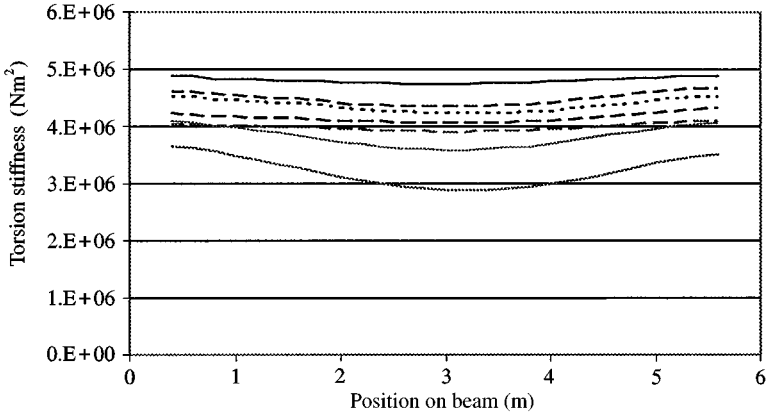

Figure 18. Dynamic torsion stiffness degradation using first torsional mode. —— Step 0; – – – Step 1; - - - Step 2; –·–·– Step 3; –··–··– Step 4; ····· Steps 5 and 6.

TABLE 2

Procentual stiffness decrease after each loadstep

		loadstep 1	loadstep 2	loadstep 3	loadstep 4	loadstep 5	loadstep 6
Global smoothing	EI	17%	21%	22%	26%	33%	48%
	GJ	10%	13%	15%	18%	26%	44%
Mindlin approach	EI	17%	21%	22%	26%	33%	49%
	GJ	8%	11%	14%	17%	24%	39%

The beam zone from 2 to 4 m (between the two pointloads) is a zone of almost constant static bending moment, which should result in the same cracking and consequently the same dynamic stiffness. Due to the weight of the beam the bending moments in the middle are slightly higher as is the degree of cracking and the reduction of the dynamic stiffness. Results from the first three bending modes are comparable.

Using the bending and torsional modes, the (averaged) decrease of stiffness in the mid-section after each static loadstep is given in Table 2 for the global smoothing and the Mindlin approach. The results for both methods are very similar. As can be observed from the dynamic stiffness degradation plots and Table 2, the first loadstep (16% of ultimate load) and the last loadstep cause the bigger decrease. The decrease in torsion stiffness is less than the decrease in bending stiffness.

Although results are similar for both methods, the possibility to enforce boundary conditions in an explicit way and the freedom to choose two parameters for smoothing the mode shapes are the advantages of the Mindlin approach compared to the global smoothing.

8. CONCLUSIONS

This paper describes a technique to determine the dynamic stiffness of a reinforced concrete beam in the undamaged and damaged state. The direct

stiffness calculation makes use of the experimental mode shapes and eigenfrequencies in order to derive the dynamic stiffness from modal curvature and torsion rate calculations. Preliminary smoothing is necessary to obtain reasonable derivatives.

The advantage of the method is that no numerical model is needed to obtain the dynamic stiffness distribution. However, a rather dense measurement grid is necessary in order to be able to identify accurately the curvatures of the higher modes.

The bending stiffness decreased with about 50% in the ultimate damaged state of the beam, the torsion stiffness with about 40%. It is noticed that bending cracks also produce a very pronounced decrease in torsion stiffness.

In the near future the dynamic bending and torsion stiffness derivation form, respectively, modal curvatures and torsion rates will be applied to a progressively damaged prestressed concrete bridge. It will be challenging to demonstrate whether damage localization and possibly quantification for a real-life structure can be obtained by the present method.

ACKNOWLEDGMENT

The experimental data used to validate the presented method comes from beam tests performed at the laboratory of the Civil Engineering Department of K.U. Leuven. They were carried out in the framework of FKFO-project No. G. 0243.96, supported by the Fleish Fund for Scientific Research.

REFERENCES

1. S. W. Doebling, C. F. Farrar, M. B. Prime and D. W. Shevitz 1996 *Research report LA-13070-MS, ESA-EA, Los Alamos National Laboratory, Los Alamos, NM,* Damage identification and health monitoring of structural and mechanical systems from changes in their vibration characteristics: a literature review.
2. F. K. Choy, R. Liang and P. Xu 1995 *Computers and Geotechnics* **17**, 57–176. Fault identification of beams on elastic foundation.
3. E. J. Williams, A. Messina and B. S. Payne 1997 *Proceedings of IMAC* **15**, 652–657, *Orlando, FL, U.S.A. February*. A frequency-change correlation approach to damage detection.
4. O. S. Salawu 1997 *Engineering Structures* **19**, 718–723. Detection of structural damage through changes in frequency: a review, Eng.
5. C. J. Carrasco, R. A. Osegueda, C. M. Ferregut and M. Grygier 1995 *Proceedings of IMAC 15*, 1786–1792, *Orlando, FL*, U.S.A. Damage localization in a space truss model using modal strain energy.
6. P. Cornwell, S. W. Doebling and C. R. Farrar 1997 *Proceedings of IMAC 15*, 1312–1318, Orlando, FL, U.S.A. February. Application of the strain energy damage detection method to plate-like structures.
7. R. Ruotolo and C. Surace 1997 *Journal of Sound & Vibration* **206**, 567–588. Damage assessment of multiple cracked beams: numerical results and experimental validation.
8. N. Stubbs and R. Osegueda 1990 *International Journal of Analytical and Experimental Modal Analysis*, **5**, 67–79. Global non-destructive damage evaluation in solids.
9. A. K. Pandey, M. Biswas and M. M. Samman 1991 *Journal of Sound & Vibration* **145**, 321–332. Damage detection from changes in curvature mode shapes.

10. C. P. Ratcliffe 1997 *Journal of Sound & Vibration* **204**, 505–517. Damage detection using a modified laplacian operator on mode shape data.
11. B. Peeters, M. Abdel Wahab, G. De Roeck, J. De Visscher, W. P. De Wilde, J.-M. Ndambi and J. Vantomme 1996 *Proceedings of ISMA21*, *Vol.* 3, *Leuven*, *Belgium*, 349–1361. Evaluation of structural damage by dynamic system identification.
12. B. Peeters, G. De Roeck, T. Pollet and L. Schueremans 1995 *Proceedings of New Advances in Modal Synthesis of Large Structures: Nonlinear*, *Damped and Nondeterministic Cases*, *Lyon*, *France*, 151–162. Stochastic subspace techniques applied to parameter identification of civil engineering structures.
13. MATLAB revision 5.2 1998 The Mathworks Inc.